IEEE Photonics Journal
An IEEE Photonics Society Publication

Optimum Integration Procedures for Supercontinuum Simulation

Volume 4, Number 2, April 2012

A. A. Rieznik
A. M. Heidt
P. G. König
V. A. Bettachini
D. F. Grosz, Member, IEEE

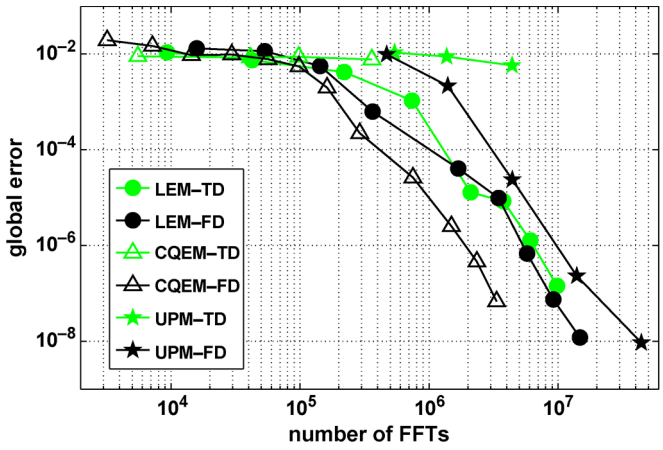

DOI: 10.1109/JPHOT.2012.2188281
1943-0655/$31.00 ©2012 IEEE

IEEE photonics SOCIETY
IEEE

Optimum Integration Procedures for Supercontinuum Simulation

A. A. Rieznik,[1,2] A. M. Heidt,[3,4] P. G. König,[1] V. A. Bettachini,[1] and D. F. Grosz,[1,2] *Member, IEEE*

[1]Instituto Tecnológico de Buenos Aires, (1106) C1033AAJ Buenos Aires, Argentina
[2]Consejo Nacional de Investigaciones Científicas y Técnicas, 7602 Stellenbosch, Argentina
[3]Laser Research Institute, University of Stellenbosch, 7602 Matieland, South Africa
[4]Institute of Photonic Technology (IPHT), 07702 Jena, Germany

DOI: 10.1109/JPHOT.2012.2188281
1943-0655/$31.00 ©2012 IEEE

Manuscript received January 13, 2012; revised February 10, 2012; accepted February 10, 2012. Date of publication February 16, 2012; date of current version April 10, 2012. This work was supported by Grant ANPCyT PICT-497/2006, Argentina. The work of A. M. Heidt was supported by the German Academic Exchange Service (DAAD). Corresponding author: V. A. Bettachini (e-mail: vbettach@itba.edu.ar).

Abstract: We study numerical solutions of the generalized nonlinear Schrödinger equation (GNLSE), focusing on the advantage of integrating the nonlinear part of the equation in the frequency domain (FD), rather than in the time domain (TD), when simulating supercontinuum generation in optical fibers. We show that integration of the nonlinear operator in the FD is more efficient than its integration in the TD. We analyze different adaptive step-size algorithms in combination with the interaction picture integration method and show that their performance strongly depends on whether integration of the nonlinear operator is performed in the FD or TD. We find that the most efficient procedure for supercontinuum simulation in optical fibers results from solving the nonlinearity in the FD and applying the recently introduced conservation quantity error adaptive step-size algorithm.

Index Terms: Fiber nonlinear optics, supercontinuum generation.

1. Introduction: Modeling and Integration Algorithms

1.1. GNLSE: Time and Frequency Domain Formulations

Fast simulation methods are required to study supercontinuum generation. Computational time becomes an even more important concern when large data sets are required. This is the case, for instance, in studies on optical rogue waves [1], where statistical approaches are used, or on dissipative soliton resonance [2], where finding the region of parameters in which these solitons exist requires an enormous number of numerical simulations. In those cases, conventional computational methods could become prohibitively slow.

Supercontinuum generation in optical fibers can be modeled through a nonlinear propagation equation that includes dispersive, Kerr, instantaneous and delayed Raman response, and self-steepening effects [3]. The common practice is to write this equation in the time domain (TD)

$$\frac{\partial A}{\partial z}+\beta_1\frac{\partial A}{\partial t}+\mathrm{i}\beta_2\frac{\partial^2 A}{\partial t^2}-\beta_3\frac{\partial^3 A}{\partial t^3}+\cdots=\mathrm{i}\gamma(\omega)\left(1+\frac{\mathrm{i}}{\omega_0}\frac{\partial}{\partial t}\right)\left(A(z,t)\int_{-\infty}^{\infty}R(t')|A(z,t-t')|^2dt'\right) \quad (1)$$

where $R(t)=(1-f_R)\delta(t)+f_R h_R(t)$, $A(z,t)$ is the electric field complex envelope, t is the retarded time for a reference frame travelling at the envelope group velocity, β_k are the usual dispersion

coefficients associated with the Taylor series expansion of the propagation constant $\beta(\omega)$ around the carrier frequency ω_0, γ is the nonlinear coefficient of the fiber fundamental mode, and $0 < f_R < 1$ represents the fractional contribution of the delayed Raman response h_R, which is usually approximated by $h_R(t) \propto \exp(-t/\tau_2)\sin(\tau_1)$. In this paper, we adopt the more accurate function

$$\begin{aligned} h_R(t) &= (f_a + f_c)h_a(t) + f_b h_b(t) \\ h_a(t) &= \tau_1\left(\tau_1^{-2} + \tau_2^{-2}\right)e^{-t/\tau_2}\sin(t/\tau_1), \quad h_b(t) = \left[(2\tau_b - t)/\tau_b^2\right]e^{-t/\tau_b} \end{aligned} \tag{2}$$

where $\tau_1 = 12.2$ fs, $\tau_2 = 32$ fs, $\tau_b = 96$ fs, $f_a = 0.75$, $f_b = 0.21$, $f_c = 0.04$, and $f_R = 0.24$ [4].

The main drawback of implementing (1) is that time derivatives lead to numerical errors due to the discretization of the time window. These derivatives vanish when transforming (1) into the frequency domain (FD), leaving only the discrete longitudinal step size as a source of numerical errors. By defining $\Omega = \omega - \omega_0$, $\tilde{A}(z,\Omega)$ as the Fourier transform of $A(z,t)$, and dropping the arguments in both $\tilde{A}(z,\Omega)$ and $A(z,t)$, the FD formulation of (1) becomes [5]

$$\frac{\partial \tilde{A}}{\partial z} + \mathrm{i}\tilde{A}(\beta(\Omega) - \beta_0 - \beta_1\Omega) = -\mathrm{i}\gamma\left(1 + \frac{\Omega}{\omega_0}\right)\left(F\left[(1 - f_R)A|A|^2 + f_R A F^{-1}\left[\tilde{h}_R F\left[|A|^2\right]\right]\right]\right) \tag{3}$$

where F stands for direct Fourier transform, F^{-1} for the inverse transform, and $\tilde{h}_R = F(h_R(t))$. Numerically, F and F^{-1} are computed using the fast Fourier transform (FFT) and inverse FFT (IFFT), respectively.

Adaptive step-size methods can be applied more successfully in the FD, as we show in the next section. Equation (3) has the additional advantage that the frequency dependence of the nonlinear coefficient $\gamma(\omega)$ can be included in straightforward fashion with the simple substitution $\gamma \to \gamma(\omega)$. This approach provides only an approximated solution but it has been shown to allow a satisfactory modeling of the frequency dependent loss, dispersion, and nonlinearity [6], [7].

1.2. Fourth-Order Runge–Kutta in the Interaction Picture Method Algorithm

The split-step Fourier method (SSFM) has been extensively used in past years to solve (1) [3], [8]–[17]. The dispersive part of the equation is solved in the FD, whereas the nonlinear part, i.e., the right-hand side (RHS) of (1), is solved in the TD. Recently, a faster integration procedure, closely related to the SSFM and originally developed for the study of Bose–Einstein condensates, was shown to be more efficient. It is called the fourth-order Runge–Kutta in the interaction picture method (RK4IPM) [15], [16]. The integration over one longitudinal step h is written as

$$\begin{aligned} A_I &= F^{-1}\left[\exp\left(\frac{h}{2}\tilde{D}\right)\tilde{A}(z,\Omega)\right], \quad k_1 = F^{-1}\left[\exp\left(\frac{h}{2}\tilde{D}\right)F[hN(A(z,t))]\right] \\ k_2 &= hN(A_I + k_1/2), \quad k_3 = hN(A_I + k_2/2), \quad k_4 = F^{-1}\left[hN\left(\exp\left(\frac{h}{2}\tilde{D}\right)F[A_I + k_3]\right)\right] \\ A(z+h,t) &= F^{-1}\left[\exp\left(\frac{h}{2}\tilde{D}\right)F[A_I + k_1/6 + k_2/3 + k_3/3]\right] + k_4/6 \end{aligned} \tag{4}$$

where $\tilde{D} = -\mathrm{i}(\beta(\Omega) - \beta_0 - \beta_1\Omega)$, and $N(A(z,t))$ is the nonlinear operator, i.e., the RHS of (1), applied to $A(z,t)$. The RK4IPM can also be applied in the FD. By defining $\tilde{N}(\tilde{A}(z,\Omega))$ as the application of the nonlinear operator in the FD, i.e., the RHS of (3), we have

$$\begin{aligned} \tilde{A}_I &= \exp\left(\frac{h}{2}\tilde{D}\right)\tilde{A}(z,\Omega), \quad k_1 = \exp\left(\frac{h}{2}\tilde{D}\right)\left(h\tilde{N}\left(\tilde{A}(z,t)\right)\right), \quad k_2 = h\tilde{N}\left(\tilde{A}_I + k_1/2\right) \\ k_3 &= h\tilde{N}\left(\tilde{A}_I + k_2/2\right), \quad k_4 = h\tilde{N}\left(\exp\left(\frac{h}{2}\tilde{D}\right)(\tilde{A}_I + k_3)\right) \\ \tilde{A}(z+h,t) &= \exp\left(\frac{h}{2}\tilde{D}\right)(\tilde{A}_I + k_1/6 + k_2/3 + k_3/3) + k_4/6. \end{aligned} \tag{5}$$

The total number of FFTs performed using (4) or (5) is 16 in both cases. The four IFFTs explicitly appearing in (4) are balanced by four additional FFTs in (5) that must be computed when implementing the nonlinear integration in the FD. An implementation of these equations in MATLAB can be found in [18]. Note that even when applying the nonlinear operator N in the TD, the convolution in the RHS of (1) is usually performed in the FD.

1.3. Adaptive Step-Size Methods

In order to optimize simulation times, the step size h can be interactively adjusted. An estimation of the error incurred at each integration step can be used to set its value. For instance, the local error method (LEM) [19] estimates the local error by taking a full step h to compute a coarse solution, then independently taking two half-steps to obtain a finer solution. The magnitude of the error can then be estimated by comparing both results. The conservation quantity error method (CQEM) [20] uses another approach. It estimates the error by calculating the photon number before and after the integration. Since (1) and (2) conserve the photon number, any deviation can be interpreted as a numerical error, and its magnitude estimated. See [20] for a description of the algorithms used to determine the step size in both LEM and CQEM.

A third method is the uncertainty principle method (UPM) [21]. Rather than estimating a local error, the UPM uses the uncertainty relation between the linear and nonlinear operators to calculate a maximum local error. The step size can then be reduced until the calculated maximum local error is arbitrarily small [21]. The main disadvantage of the UPM is that it only works with generalized nonlinear Schrödinger equations (GNLSEs) with Hermitian nonlinear operators, which is not the case in (1) and (3). Nonetheless, we estimated the maximum error by only considering the imaginary part of the nonlinear operator. This assumption works for moderate-power regimes, but as we show next, its performance degrades when high powers are considered.

2. Results

We assess the efficiency of the TD or FD integration of the nonlinear operator N by modeling supercontinuum generation in optical fibers. We explored a wide range of system parameters and show results for two representative cases. Simulation parameters are those of [20], representing the propagation of femtosecond pulses in the anomalous dispersion region of a highly nonlinear photonic crystal fiber (PCF). The fiber zero-dispersion wavelength is 780 nm, and the corresponding dispersion coefficients were taken from [3]. The input pump pulse is centered at 835 nm with a hyperbolic-secant profile $A(0,t) = \sqrt{P}\mathrm{sech}(t/t_0)$, where $t_0 = 28.4$ fs, $P = 10$ kW (first case), and $P = 50$ kW (second case). The propagation distance is 10 cm. Output spectra, obtained using (5), for both cases are shown in Fig. 1. We use a time window of 32 ps and 2^{15} samples.

Fig. 2 illustrates, for $P = 10$ kW, the efficiency of the six approaches studied in this paper. We find the solution using TD or FD integration of the nonlinear operator and in each case test the LEM, CQEM and UPM for the adaptive adjustment of h. To compare results, we calculate the global error ε for each simulation, which is defined as [22]

$$\varepsilon = \sum_{k=1}^{N} \frac{\left| |A_k^{\mathrm{sim}}|^2 - |A_k^{\mathrm{true}}|^2 \right|}{N \max\left(|A_k^{\mathrm{true}}|^2 \right)} \tag{6}$$

where n is the number of field samples, A^{sim} is the simulated field at the output of the PCF, and A^{true} is a reference solution obtained at the highest achievable numerical precision. Note, however, that this definition of the global error, which has also been adopted in [20] and [22], is insensitive to phase errors. As such, we verified the convergence of our simulations adopting an alternative global error definition that takes into account phase errors [22] and obtained similar results.

We verified that simulation results do not depend on which method is used to obtain A^{true} as long as the same precision is reached and the same implementation in TD or FD is used (see Section 3.1 for further discussion). The number of FFTs performed in a given simulation is used as a measure of

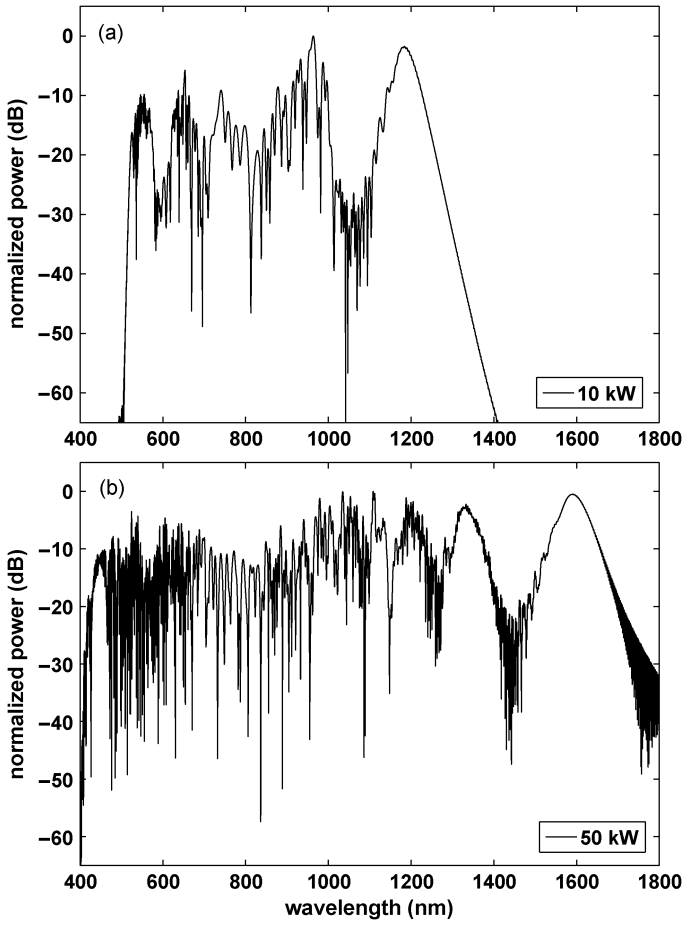

Fig. 1. Simulated output spectra. (a) $P = 10$ kW. (b) $P = 50$ kW. See the text for simulation parameters.

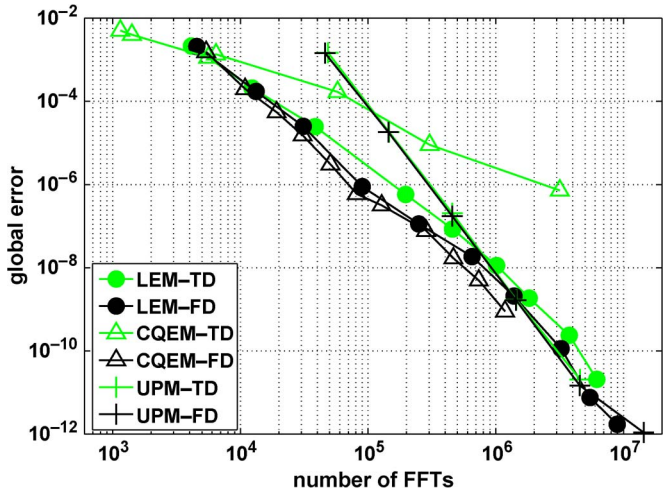

Fig. 2. Simulation global error versus number of FFTs using six different approaches: LEM, CQEM, and UPM solving the nonlinear operator in either time or frequency domain, for an input pulse peak power of 10 kW.

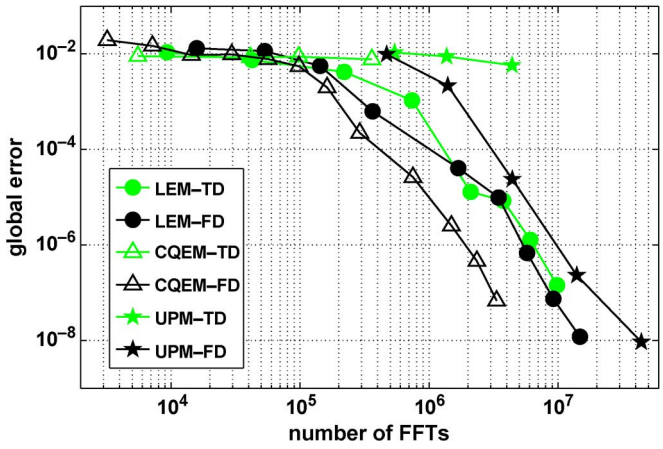

Fig. 3. Simulation global error versus number of FFTs using all six approaches. Input parameters are the same as those in Fig. 2, but the input pulse peak power is 50 kW.

its computational cost, as done in previous publications [19], [21]. We verified that this number is proportional to the simulation time (see Section 3.4 for further explanation).

Fig. 2 illustrates that the different methods show similar computational performance for $P = 10$ kW. The application of the FD approach in (5) together with the CQEM (CQEM-FD) is the most effective method, in the sense that it requires fewer FFTs to achieve a given global error. When the nonlinear integration is performed in TD, the LEM is the most efficient method until the accuracy reaches a value of 10^{-8}. For higher accuracies, i.e., for smaller global errors, the UPM performs better. The CQEM is not suitable for TD calculations.

For $P = 50$ kW, Fig. 3 shows the same trends as in Fig. 2, but the difference in performance is more dramatic. In the FD and for acceptable global errors (smaller than 10^{-3}), the CQEM achieves approximately an order of magnitude higher accuracy than the LEM for the same number of FFTs. These results confirm the observation in [20] that the CQEM performs better for more complex problems.

The upper limit to the curves in these figures, which is always around 10^{-2}, is determined by the highest possible target value imposed to the local error, above which simulations no longer converge. This limits the minimum number of FFTs that a given method requires to achieve convergence. For instance, the UPM-FD and UPM-TD need $4 \cdot 10^2$ FFTs to reach a global error of 10^{-2} (see Fig. 3) and when one attempts to perform less FFTs, by decreasing the target local error, the field diverges.

We also observe that for $P = 50$ kW, the LEM is far more efficient than the UPM, for a given global error, when nonlinear integration is carried out in the TD. For the higher peak power even the CQEM-TD is more efficient than the UPM-TD. We attribute this to the fact that, for higher peak powers, the real part of the nonlinear operator cannot be neglected and the approximation made in the implementation of the UPM no longer holds.

3. Discussion

3.1. FD versus TD Integration

The TD formulation of the GNLSE (1) contains time derivatives, which can only be calculated approximately in the discrete numerical case with a finite number of sample points. Therefore, additional derivative-related numerical errors are introduced, which are independent of the longitudinal step size and cannot be minimized by an adaptive step-size algorithm. The calculation of time derivatives can be avoided transforming the GNLSE into the FD (3). Since the only remaining source for numerical errors is the finite step size, which can be efficiently controlled by adaptive methods, it is to be expected that any of these methods will perform better in the FD. This is

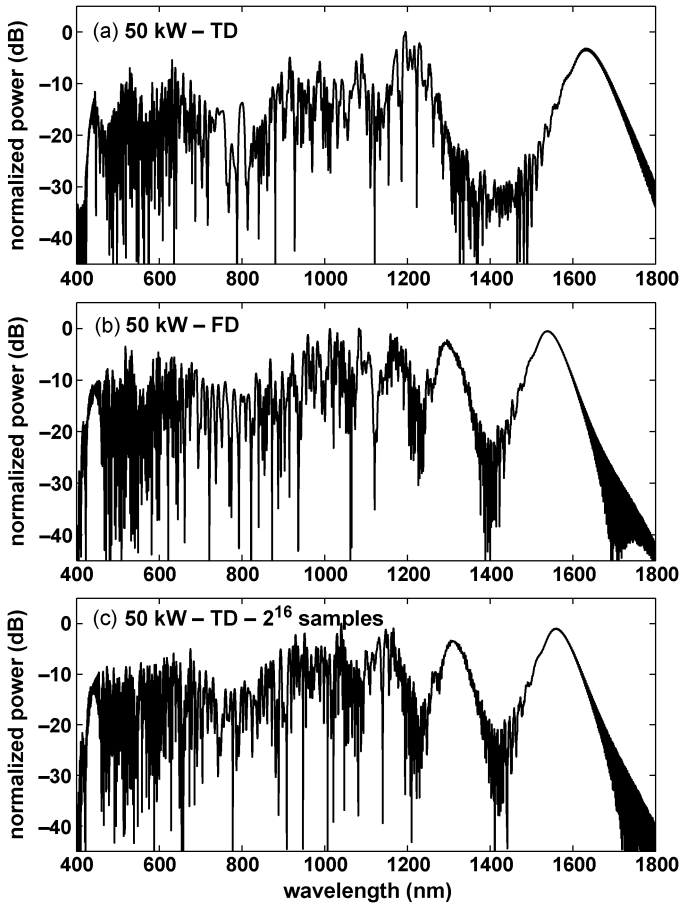

Fig. 4. Simulated output spectra. (a) $P = 50$ kW, with 2^{15} sample points, using TD integration, (b) $P = 50$ kW, 2^{15} points, FD integration, and (c) $P = 50$ kW, 2^{16} points, TD integration. Other simulation parameters can be found in the text.

confirmed in our simulations, as shown in Figs. 2 and 3. FD implementations of all investigated adaptive step-size methods perform more efficient than their TD counterparts, with the exception of one case (using LEM-TD) in Fig. 3. However, the performance difference between TD and FD implementation varies significantly for the investigated methods. This way, it is important to select the correct adaptive method for a given implementation: a point discussed in Section 3.2.

There is another consequence of solving the GNLSE in the FD. Solutions found in TD and FD are not identical. This means that the reference solution A^{true}, calculated at the highest numerical precision for the longitudinal step size, is different for TD and FD implementations. For $P = 10$ kW, this difference was found to be very small, i.e., the spectrum shown in Fig. 1 is nearly identical either using TD or FD nonlinear integration. On the other hand, for $P = 50$ kW the difference is dramatic, as shown in Fig. 4. This is due to the fact that (1) is a 2-D problem. Even if the error in z is minimized, the derivative-related errors in t remain the same, since the number of samples is kept constant. Therefore, due to the approximate nature of numerical calculations of derivatives, the solution found in the TD is basically less accurate than the solution found in the FD. If the time resolution is increased, either by using a larger number of sampling points or a smaller time window, the accuracy in the derivatives calculations increases as well, and the TD solution converges towards the solution found in the FD (with less sampling points) as shown in Fig. 4(b). When the number of samples is increased to 2^{16}, keeping the total time window of 32 ps, TD integration produces the same spectrum as FD integration [see Fig. 4(c)]. However, the additional sampling points are associated with a severe increase in computational cost. If highly accurate solutions are

required, it is therefore advisable to work entirely in the FD. For our error calculations in (6), we used a separate A^{true} for time and frequency implementations to ensure a fair comparison of the adaptive step-size methods, because these methods are only able to minimize the error in the propagation direction and should not be evaluated based on inherent errors of the particular implementation.

3.2. Optimum Adaptive Step-Size Method for TD or FD Integrations

If (4) is applied, i.e. the nonlinear operator is solved in TD as it is usually done, the LEM is much more efficient than the CQEM. We attribute this to the fact that the CQEM is sensitive to errors introduced by the calculation of numerical derivatives in the TD solution of N, as these errors change the photon number. As such, the algorithm keeps the step size small in order to compensate, but since errors are not related to the finite step size, this behavior leads, in fact, to a worse performance. In contrast, the LEM is only sensitive to errors introduced by the discrete step size, and therefore performs more efficiently if there are other errors present which are not step-size related.

3.3. CQEM Disadvantages

We note that the smallest global error the CQEM can achieve is limited even when the nonlinear integration is performed in the FD. In Figs. 2 and 3, the CQEM-FD does not reach global errors smaller than 10^{-8} and 10^{-7}, respectively. When we tried to reach higher accuracies by imposing a smaller limit to the photon number mismatch after each integration step, the simulation stopped. This limitation is due to the fact that calculations in the default MATLAB package use double precision numbers which are accurate to the 15th digit, whereas to obtain smaller global errors through the CQEM-FD relative photon number errors smaller than 10^{-15} are necessary. For these calculations, the default MATLAB package is not accurate enough and therefore the CQEM algorithm reduces the step size in an endless loop.

In principle, one can solve this problem by either using a larger precision programming language or including additional multiple precision toolboxes into MATLAB, but this is certainly a limit to the CQEM-FD. In practice, however, one rarely requires such small global errors.

A second drawback of the CQEM-FD appears when we look at the local versus global error and perform a linear fit. Ideally, the slope of this curve should be 1, indicating that the global error accuracy could be improved by simply setting a proportional change in the tolerated local error [19], [21]. In Fig. 5, we show these plots for the two most efficient integration procedures, i.e., CQEM-FD and LEM-FD. It is clear that the LEM-FD produces slopes closer to 1.

3.4. FFT as a Measure of Computational Cost

A natural question related to Figs. 2 and 3 is whether the number of FFTs represents a good measure of computational cost or simulation time. This is the case for large values of sample points n, since it is well known that each FFT performs between $4n\log_2(n)$ to $5n\log_2(n)$ arithmetical operations, depending on the implemented algorithm [20], whereas the number of all other operations in any of the methods grows linearly with n.

As stated before, we used $n = 2^{15}$ samples. To check this point, we divided the simulation time in our computer by the number of FFTs for each simulation. The CQEM-FD and LEM-FD give the same value (0.011 s/FFT), whereas the UPM-FD gives a slightly higher value (0.013 s/FFT). This indicates that if we plotted results against simulation time instead of number of FFTs, the LEM-FD and CQEM-FD would show the same behavior, whereas the UPM-FD would perform slightly worse than shown in Figs. 2 and 3. The same result holds for simulations using TD nonlinear integration. We then choose the number of FFTs as a measure of computational cost because it can be reproduced easily, whereas the simulation time depends on the particular hardware and software conditions. Our codes are open to the community in order to facilitate reproduction of the results presented in this paper [18].

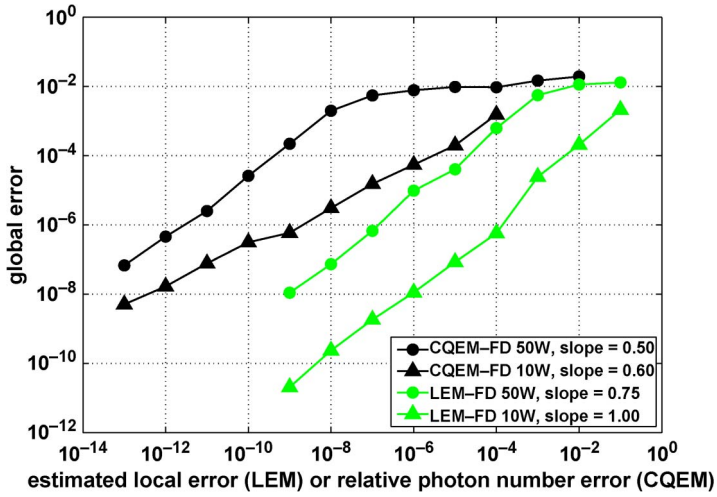

Fig. 5. Global error of the simulation versus estimated local error (LEM) or relative photon number error (CQEM) for the two most efficient methods, namely, CQEM-FD and LEM-FD, and for 10 and 50 kW input peak power. We also show in the legend each curve linear fitting slope.

4. Conclusion

As mentioned above, solutions to the GNLSE with nonlinearity dispersion are naturally computed in the FD. In this case, both LEM and CQEM have been successfully employed for the step-size adaptation [6], [14], [23]. In this paper, we showed that the use of the FD approach integration is advisable, even when the nonlinear coefficient is taken to be constant over the spectral bandwidth, as the numerical solution in the FD is inherently more accurate and faster, for a given acceptable global error, than the TD approach.

As pointed out in Section 1.1, to consider nonlinearity dispersion, the use of (3) with the substitution $\gamma \rightarrow \gamma(\omega)$, has been commonly employed. This, however, is an ad hoc procedure, and a proper derivation requires a generalization of the effective-area concept. To this purpose, a new equation is rigorously derived in [6]. As it has the same form as (3), the results presented in this paper remain valid.

References

[1] D. R. Solli, C. Ropers, P. Koonath, and B. Jalali, "Optical rogue waves," *Nature*, vol. 450, no. 7172, pp. 1054–1057, Dec. 2007.
[2] P. Grelu, W. Chang, A. Ankiewicz, J. M. Soto-crespo, and N. Akhmediev, "Dissipative soliton resonance as a guideline for high-energy pulse laser oscillators," *J. Opt. Soc. Amer. B*, vol. 27, no. 11, pp. 2336–2341, Nov. 2010.
[3] J. M. Dudley, G. Genty, and S. Coen, "Supercontinuum generation in photonic crystal fiber," *Rev. Mod. Phys.*, vol. 78, no. 4, pp. 1135–1184, Oct. 2006.
[4] Q. Lin and G. P. Agrawal, "Raman response function for silica fibers," *Opt. Lett.*, vol. 31, no. 21, p. 3086, Nov. 2006.
[5] P. L. François, "Nonlinear propagation of ultrashort pulses in optical fibers: Total field formulation in the frequency domain," *J. Opt. Soc. Amer. B*, vol. 8, no. 2, p. 276, Feb. 1991.
[6] J. Laegsgaard, "Mode profile dispersion in the generalised nonlinear Schrödinger equation," *Opt. Exp.*, vol. 15, no. 24, pp. 16 110–16 123, Nov. 2007.
[7] V. Pureur and J. M. Dudley, "Nonlinear spectral broadening of femtosecond pulses in solid-core photonic bandgap fibers," *Opt. Lett.*, vol. 35, no. 16, pp. 2813–2815, Aug. 2010.
[8] S. Roy, S. K. Bhadra, and G. P. Agrawal, "Perturbation of higher-order solitons by fourth-order dispersion in optical fibers," *Opt. Commun.*, vol. 282, no. 18, pp. 3798–3803, Sep. 2009.
[9] A. Podlipensky, P. Szarniak, N. Y. Joly, C. G. Poulton, and P. S. J. Russell, "Bound soliton pairs in photonic crystal fiber," *Opt. Exp.*, vol. 15, no. 4, pp. 1653–1662, Feb. 2007.
[10] G. Genty, M. Lehtonen, H. Ludvigsen, J. Broeng, and M. Kaivola, "Spectral broadening of femtosecond pulses into continuum radiation in microstructured fibers," *Opt. Exp.*, vol. 10, no. 20, pp. 1083–1098, Oct. 2002.
[11] I. Cristiani, R. Tediosi, L. Tartara, and V. Degiorgio, "Dispersive wave generation by solitons in microstructured optical fibers," *Opt. Exp.*, vol. 12, no. 1, pp. 124–135, Jan. 2004.

[12] K. M. Hilligse, T. V. Andersen, H. N. Paulsen, C. K. Nielsen, K. Mlmer, S. Keiding, R. Kristiansen, K. P. Hansen, and J. J. Larsen, "Supercontinuum generation in a photonic crystal fiber with two zero dispersion wavelengths," *Opt. Exp.*, vol. 12, no. 6, pp. 1045–1054, Mar. 2004.
[13] M. H. Frosz, P. Falk, and O. Bang, "The role of the second zero-dispersion wavelength in generation of supercontinua and bright-bright soliton-pairs across the zero-dispersion wavelength," *Opt. Exp.*, vol. 13, no. 16, pp. 6181–6192, Aug. 2005.
[14] J. C. Travers, A. B. Rulkov, B. A. Cumberland, S. V. Popov, and J. R. Taylor, "Visible supercontinuum generation in photonic crystal fibers with a 400 W continuous wave fiber laser," *Opt. Exp.*, vol. 16, no. 19, pp. 14 435–14 447, Sep. 2008.
[15] M. E. Masip, A. A. Rieznik, P. G. König, D. F. Grosz, A. V. Bragas, and O. E. Martínez, "Femtosecond soliton source with fast and broad spectral tunability," *Opt. Lett.*, vol. 34, no. 6, pp. 842–844, Mar. 2009.
[16] G. P. Agrawal, *Nonlinear Fiber Optics*. New York: Academic, 2007.
[17] T. R. Taha and M. I. Ablowitz, "Analytical and numerical aspects of certain nonlinear evolution equations. ii. numerical, nonlinear Schrödinger equation," *J. Comput. Phys.*, vol. 55, no. 2, pp. 203–230, Aug. 1984.
[18] A. A. Rieznik, "Free optics project," in *Website*, 2010, see the Free Downloads section. [Online]. Available: www.freeopticsproject.org
[19] O. V. Sinkin, R. Holzlöhner, J. Zweck, and C. R. Menyuk, "Optimization of the split-step Fourier method in modeling optical-fiber communications systems," *J. Lightwave Technol.*, vol. 21, no. 1, pp. 61–68, Jan. 2003.
[20] A. Heidt, "Efficient adaptive step size method for the simulation of supercontinuum generation in optical fibers," *J. Lightwave Technol.*, vol. 27, no. 18, pp. 3984–3991, Sep. 2009.
[21] A. Rieznik, T. Tolisano, F. A. Callegari, D. Grosz, and H. Fragnito, "Uncertainty relation for the optimization of optical-fiber transmission systems simulations," *Opt. Exp.*, vol. 13, no. 10, pp. 3822–3834, May 2005.
[22] J. Hult, "A fourth-order Runge–Kutta in the interaction picture method for simulating supercontinuum generation in optical fibers," *J. Lightwave Technol.*, vol. 25, no. 12, pp. 3770–3775, Dec. 2007.
[23] A. M. Heidt, "Pulse preserving flat-top supercontinuum generation in all-normal dispersion photonic crystal fibers," *J. Opt. Soc. Amer. B*, vol. 27, no. 3, pp. 550–559, Mar. 2010.